Effects of cold rolling deformation on microstructure, hardness, and creep behavior of high nitrogen austenitic stainless steel*

Sun Shi-Cheng(孙世成)[a)b)], Sun Gui-Xun(孙贵训)[a)], Jiang Zhong-Hao(江忠浩)[a)†], Ji Chang-Tao(季长涛)[b)‡], Liu Jia-An(刘家安)[a)], and Lian Jian-She(连建设)[a)]

[a)] *Key Laboratory of Automobile Materials, College of Materials Science and Engineering, Jilin University, Nanling Campus, Changchun* 130025, *China*
[b)] *Key Laboratory of Advanced Structural Materials, Ministry of Education, College of Materials Science and Engineering, Changchun University of Technology, Changchun* 130012, *China*

(Received 7 August 2013; revised manuscript received 23 October 2013; published online 20 December 2013)

Effects of cold rolling deformation on the microstructure, hardness, and creep behavior of high nitrogen austenitic stainless steel (HNASS) are investigated. Microstructure characterization shows that 70% cold rolling deformation results in significant refinement of the microstructure of this steel, with its average twin thickness reducing from 6.4 μm to 14 nm. Nanoindentation tests at different strain rates demonstrate that the hardness of the steel with nano-scale twins (nt-HNASS) is about 2 times as high as that of steel with micro-scale twins (mt-HNASS). The hardness of nt-HNASS exhibits a pronounced strain rate dependence with a strain rate sensitivity (m value) of 0.0319, which is far higher than that of mt-HNASS (m = 0.0029). nt-HNASS shows more significant load plateaus and a higher creep rate than mt-HNASS. Analysis reveals that higher hardness and larger m value of nt-HNASS arise from stronger strain hardening role, which is caused by the higher storage rate of dislocations and the interactions between dislocations and high density twins. The more significant load plateaus and higher creep rates of nt-HNASS are due to the rapid relaxation of the dislocation structures generated during loading.

Keywords: high nitrogen austenitic stainless steel, cold deformation, nanoindentation tests, creep behavior

PACS: 61.82.Bg, 81.40.Ef, 62.90.+k, 62.20.Hg **DOI:** 10.1088/1674-1056/23/2/026104

1. Introduction

High nitrogen austenitic stainless steels (HNASSs) (whose nitrogen concentration is higher than 0.4% in mass percent[1]) are becoming an increasingly important new class of polycrystalline engineering materials due to the fact that they possess lots of attractive mechanical properties, such as high strength and ductility, desirable toughness, high work hardening ability, and excellent corrosion resistance compared with the conventional austenitic stainless steels.[2–8] These properties greatly depend on the nitrogen in solid solution. The solubility of nitrogen increases as the manganese and chromium content increases; therefore, nitrogen alloying could be effectively used in the alloy system of Cr–Mn.[9] Interstitial nitrogen is very effective for solid-solution strengthening[10,11] and for stabilizing the austenitic structure. The high austenitizing capacity of nitrogen makes it possible to replace expensive nickel, which offers an additional advantage of cost-saving. These properties make the investigations of HNASS of great significance. Thus, the mechanical properties and microstructure evolution of HNASS have been intensively studied.[12–17]

Cold rolling can greatly influence the microstructure and, hence, ultimately determine the mechanical properties. Large amounts of work on cold rolling deformation of HNASS has been reported[5,16,18–20] and deformation twins and slip lines have been found in the cold rolling plastic deformation of HNASS.[5,21,22] Cold rolling can generate severe plastic deformation, which is also an effective way to perform grain size refinement.[16,23] However, phase transformation hardly happens in HNASS due to the high austenitizing capacity of nitrogen, even at cryogenic temperature or after severe cold deformation.[24,25] Despite this, most studies about HNASS only have a small cold rolling deformation. The effect of large cold rolling deformation, particularly the effects of cold rolling deformation on the microstructure, hardness, and creep behavior of HNASS, have not yet been investigated.

A primary aim of this study is to investigate the effects of cold rolling deformation on microstructure, hardness, and creep behavior of HNASS. Detailed microscopy investigations are performed by electron backscattering diffraction (EBSD) and transmission electron microscopy (TEM). The hardness and creep behaviors are examined by performing nanoindentation tests loading in a broad loading strain rate range.

2. Experiment

The HNASS use in this study was produced by Institute of High Nitrogen Steel, Changchun University of Technology. The nominal chemical compositions of the HNASS in this

*Project supported by the National Natural Science Foundations of China (Grant Nos. 51371089 and 51201068) and the National Key Basic Research and Development Program of China (Grant No. 2010CB631001).

†Corresponding author. E-mail: jzh@jlu.edu.cn
‡Corresponding author. E-mail: jichangtao@mail.ccut.edu.cn

© 2014 Chinese Physical Society and IOP Publishing Ltd

test are shown in Table 1. The ingots were initially solution-treated at 1150 °C for 8 h followed by water quenching in order to keep nitrogen in solid solution. Subsequently, the ingots (70×20 mm), each of which was 20-mm thick, were cold rolled on a laboratory two-high mill. The mill was set to give about 0.2-mm thick reduction per pass at room temperature (without any heat treatment). Sheets with a thickness reduction of 70% were obtained. The HNASS after solution treatment was referred to as mt-HNASS, and HNASS after cold rolling was named nt-HNASS. Here, the nt-HNASS has the same chemical compositions as the mt-HNASS.

Table 1. Chemical compositions of the HNASS in this test (mass percent, %).

C	N	Cr	Mn	Mo	Si	Nb	P	S	Fe
0.02	0.83	22	17	2.43	0.27	0.21	0.012	0.004	balance

The microstructures of the samples were characterized by TEM (JEM-2100F) with an accelerating voltage of 200 kV. The crystallographic structures were investigated by EBSD using a field emission scanning electron microscopy (FESEM, SUPRA-40). The data obtained by the EBSD method were analyzed by orientation imaging microscopy (OIM^{TM}). The discrete step size used for EBSD mapping ranged from 10 nm to 100 nm. Thin foil samples for the TEM and EBSD observation were prepared by ion beam thinning using the Ion Polishing System (Gantan 691, USA), with a voltage of 5 kV and a tilt angle of 6°.

The nanoindentation tests were carried out on an Agilent Nanoindenter G200 System that was equipped with a diamond Berkovich-type (three-sided pyramid) indenter at room temperature. The HNASS samples were first indented at constant loading strain rates in a range from $4\times10^{-3}/\mathrm{s}$ to $4\times10^{-1}/\mathrm{s}$ to a maximum displacement of 2000 nm. Then, the samples were held at the maximum load for different times (dwell period). Finally, the samples were unloaded to 10% of the maximum load at the same unloading strain rate. An indentation test was made at least ten times for each loading strain rate. Prior to the nanoindentation tests, the mt-HNASS and nt-HNASS were mechanically ground and polished in order to achieve clean and smooth test surfaces.

3. Results and discussion

Figures 1(a) and 1(b) show the representative load–displacement (P–h) curves obtained from the nanoindentation tests for the mt-HNASS and nt-HNASS, respectively. The curves in both materials are obtained at a maximum indenter displacement of 2000 nm and holding time of 1200 s in seven different values of loading strain rate ($\dot{\varepsilon}_{\mathrm{L}}$). A higher load is required in order to impose the same indenter displacement with the increasing of $\dot{\varepsilon}_{\mathrm{L}}$ for mt-HNASS and nt-HNASS in the loading regime. This trend of the loading strain rate dependence is similar to that of the Cu with nano-scale twins.[26–28] The load imposed on the nt-HNASS is also considerably larger than that on the mt-HNASS for a given indenter displacement in the nanoindentation tests. It can be seen from Fig. 1 that the load increases more sharply to a given indenter displacement for nt-HNASS than for mt-HNASS with the increase of $\dot{\varepsilon}_{\mathrm{L}}$ in the loading regime. This phenomenon indicates a significant strain rate sensitivity of nt-HNASS compared with that of mt-HNASS, which can be determined by the strain rate sensitivity ($m=\partial\log H/\partial\log\dot{\varepsilon}_{\mathrm{L}}$),[29] where H is the hardness and $\dot{\varepsilon}_{\mathrm{L}}$ is the loading strain rate.

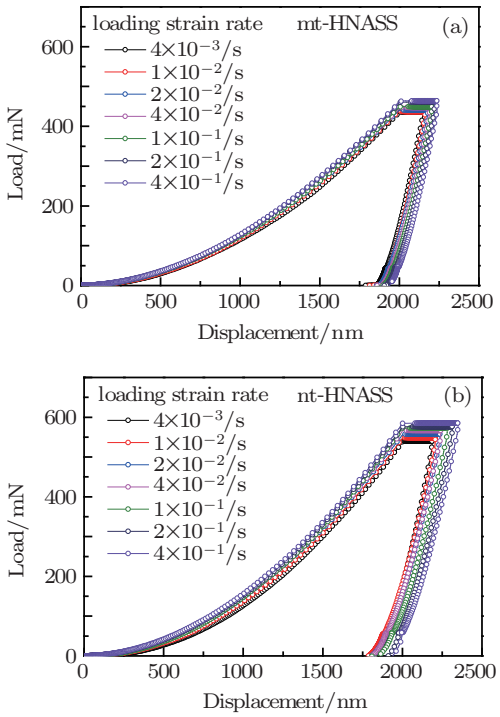


Fig. 1. (color online) Load–displacement (P–h) curves obtained at a maximum indenter displacement of 2000 nm and a holding time of 1200 s for different loading strain rates for the mt-HNASS (a) and nt-HNASS (b).

In order to obtain a more accurate hardness, nanoindentation tests were performed at room temperature in the same range of $\dot{\varepsilon}_{\mathrm{L}}$ to the same displacement as those above but held for a short time (200 s). Variations of hardness with loading strain rate in the logarithm form of mt-HNASS and nt-HNASS are shown in Fig. 2(a). As shown in Fig. 2(a), the hardness of nt-HNASS is about two times as high as that of mt-HNASS. Figure 2(b) shows the corresponding double logarithmic curves of hardness versus loading strain rate ($\log H-\log\dot{\varepsilon}_{\mathrm{L}}$) obtained for mt-HNASS and nt-HNASS. As shown in Fig. 2(b), the m value of mt-HNASS is 0.0029 and the m value is 0.0319 for nt-HNASS. These values are still far below than that of grain boundary (GB) sliding ($m=0.5$)[30] or Coble creep ($m=1.0$).[21,31] Another phenomenon observed from the present nanoindentation tests is that the m of nt-HNASS is one order of magnitude as high as that of mt-HNASS.

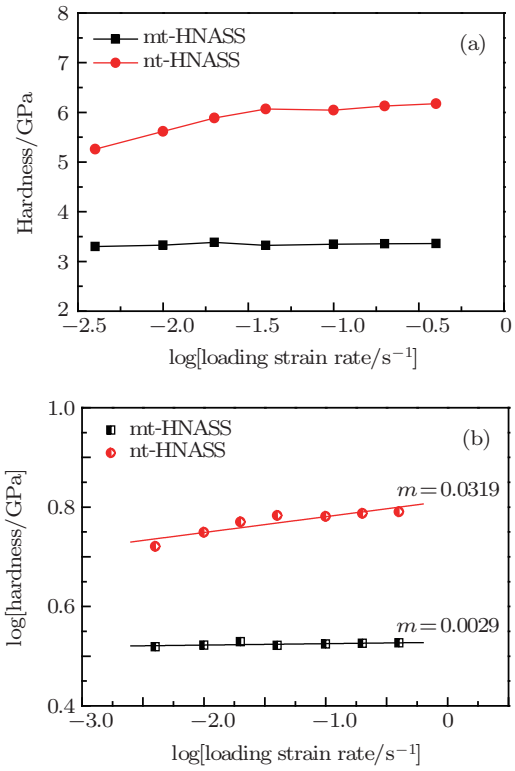


Fig. 2. (color online) Variations of hardness with loading strain rate in the logarithm form (a) and corresponding double logarithmic form ($\log H$–$\log \dot{\varepsilon}_{\rm L}$) (b) at a holding time of 200 s.

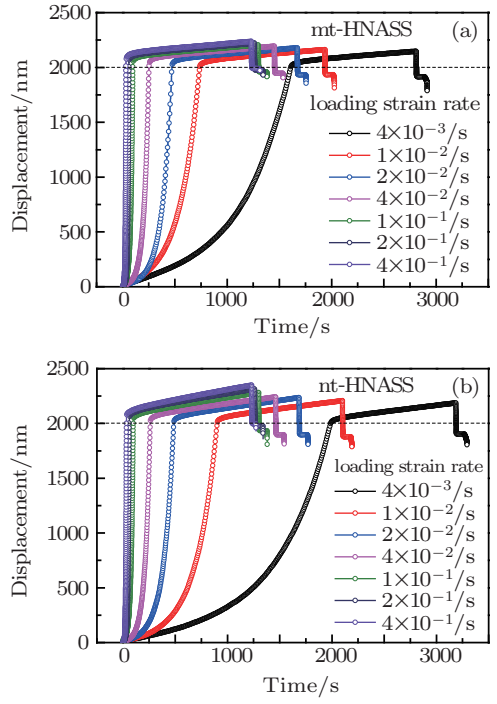


Fig. 3. (color online) Displacement–time (h–t) curves obtained at an indenter displacement of 2000 nm and a holding time of 1200 s for different loading strain rates for the mt-HNASS (a) and nt-HNASS (b).

As shown in Fig. 1, the P–h curves exhibit significant load plateaus at higher values of $\dot{\varepsilon}_{\rm L}$ in the holding regime. Such a variation of load plateaus indicates that there is an increase in indenter displacement or a significant creep deformation with an increase in $\dot{\varepsilon}_{\rm L}$ in the holding regime, which can also be seen in the corresponding displacement–time (h–t) curves (Fig. 3) obtained for mt-HNASS and nt-HNASS at seven different loading strain rates ranging from 4×10^{-3}/s to 4×10^{-1}/s.

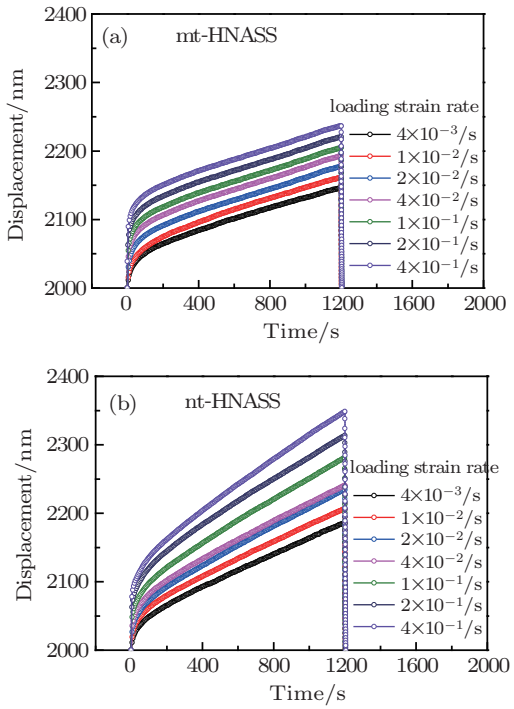


Fig. 4. (color online) Displacement–time (h–t) curves obtained at an indenter displacement of 2000 nm and a holding time of 1200 s for different loading strain rates in the holding and unloading regimes for the mt-HNASS (a) and nt-HNASS (b).

The widths of the load plateaus or the indenter displacement increase monotonically with the increase of $\dot{\varepsilon}_{\rm L}$. They reach a maximum value of ~ 250 nm at $\dot{\varepsilon}_{\rm L} = 4 \times 10^{-1}$/s for mt-HNASS and a maximum value of $\sim$348 nm at $\dot{\varepsilon}_{\rm L} = 4 \times 10^{-1}$/s for nt-HNASS. In order to evaluate the creep deformation observed above, the h–t curves in the holding and unloading regimes, which are taken from Fig. 3, are plotted in Fig. 4 each as a function of time. Then, the values of creep strain ($\varepsilon_{\rm H} = {\rm d}h/h$) could be determined by using the h–t data in the holding regime in Fig. 4, which are plotted in Fig. 5, each as a function of holding time. By differentiating the $\varepsilon_{\rm H}$–t curves in Fig. 5, the creep strain rate ($\dot{\varepsilon}_{\rm H} = ({\rm d}h/{\rm d}t)/h$) can also be derived, which are plotted in Fig. 6, each as a function of holding time. As shown in Figs. 5 and 6, there is an initial transition regime in which $\varepsilon_{\rm H}$ rises rapidly and the corresponding $\dot{\varepsilon}_{\rm H}$ drops off rapidly with the increasing holding time. Then, a steady-state creep deformation process occurs after a holding time of ~ 10 s, in which the $\varepsilon_{\rm H}$ increases slowly and the corresponding $\dot{\varepsilon}_{\rm H}$ decreases stably with the increase in holding time. Both $\varepsilon_{\rm H}$ and $\dot{\varepsilon}_{\rm H}$ increased with the increase in $\dot{\varepsilon}_{\rm L}$ at a given holding time. At a holding time of 1200 s, the largest $\varepsilon_{\rm H}$ at $\dot{\varepsilon}_{\rm L} = 4 \times 10^{-1}$/s for nt-HNASS is $\sim 14.8\%$,

which is ~ 1.3 times as high as that for the mt-HNASS at $\dot{\varepsilon}_L = 4 \times 10^{-1}$/s and $\sim$1.7 times as high as the lowest loading strain rate ($\dot{\varepsilon}_L = 4 \times 10^{-3}$/s) for nt-HNASS. At zero holding time, the highest $\dot{\varepsilon}_H$ at $\dot{\varepsilon}_L = 4 \times 10^{-1}$/s for nt-HNASS is $\sim 2 \times 10^{-2}$/s, which is $\sim$2 times as high as that for the mt-HNASS at $\dot{\varepsilon}_L = 4 \times 10^{-1}$/s and ~ 7.5 times as high as the lowest loading strain rate ($\dot{\varepsilon}_L = 4 \times 10^{-3}$/s) for nt-HNASS.

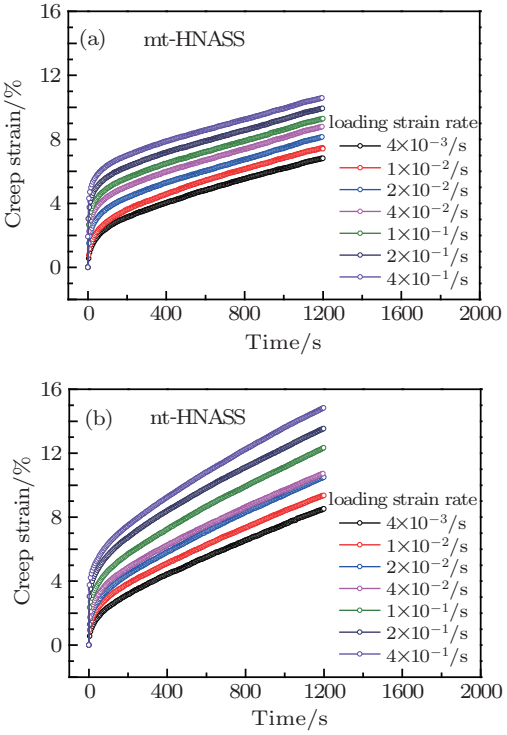


Fig. 5. (color online) Variations of the creep strain with holding time obtained at an indenter displacement of 2000 nm and a holding time of 1200 s for different loading strain rates in the holding regimes for the mt-HNASS (a) and nt-HNASS (b).

Under a constant load, an increase in indenter displacement corresponds to an increase in the contact area of the indenter tip/sample and, thus, a decrease in hardness or stress. According to the relationship of $H = P/(ch^2)$,[32] a simple equation for the stress (σ_H) can be derived in the holding regime, that is $\sigma_H = (H/3)(h_0/h)^2$, where H is the hardness, P is the load, h is the contact displacement, c is a constant that depends on the geometry of the indenter (24.56 for the perfect Berkovich geometry), and h_0 is the maximum indenter displacement imposed in the loading regime ($h_0 = 2000$ nm). From this expression and the experimental h–t data in Fig. 4, σ_H can be calculated and the corresponding σ_H–t curves are plotted in Fig. 7, each as a function of holding time. It can be seen that an initial transition regime exists in which σ_H drops off rapidly as the holding time increases. And, after a holding time of ~ 10 s, the σ_H drops off slowly as holding time increases.

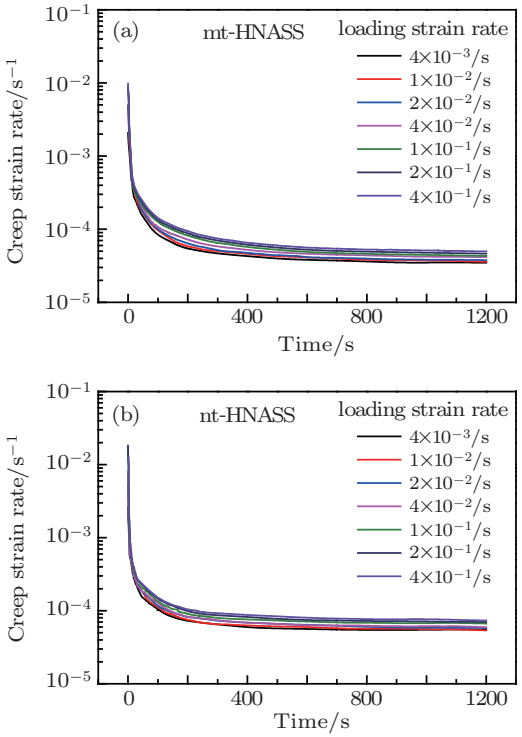


Fig. 6. (color online) Variations of the creep strain rate with holding time obtained at an indenter displacement of 2000 nm and a holding time of 1200 s for different loading strain rates in the holding regimes for the mt-HNASS (a) and nt-HNASS (b).

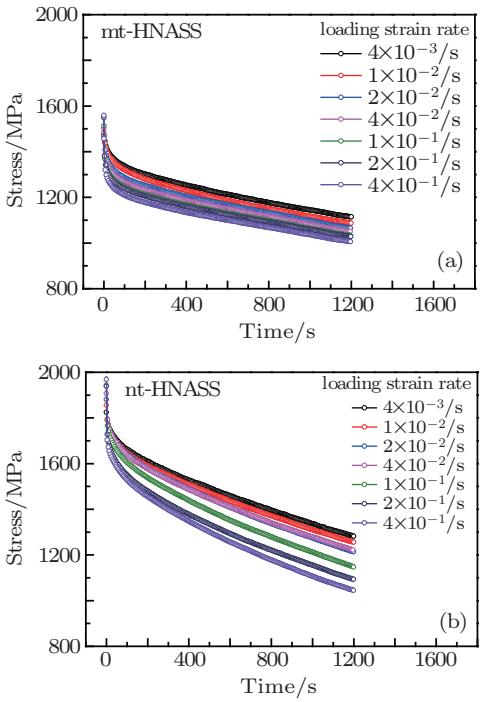


Fig. 7. (color online) Variations of the stress with holding time obtained at an indenter displacement of 2000 nm and a holding time of 1200 s for different loading strain rates in the holding regimes for the mt-HNASS (a) and nt-HNASS (b).

The typical inverse pole figure (IPF) color maps of EBSD in Figs. 8(a) and 8(b) are selected from a large number of EBSD observations. These two figures show that there are

significant differences in orientation between mt-HNASS and nt-HNASS before nanoindentation tests, which depend on their crystallographic orientation components. The crystallographic orientations on the observed surface are displayed by the colors shown in the stereographic triangle superimposed in Fig. 8(b). As shown in Fig. 8(a), the microstructure of mt-HNASS is composed of equiaxed grains with random crystalline orientations and predominant high-angle GBs. The twins formed during the solution treatment process are visible in the overwhelming majority of grains. There is no texture in mt-HNASS. It is found that the average twin thickness is about 6.4 μm and the average grain size is about 30 μm for mt-HNASS from statistical measurements. The microstructure of nt-HNASS is shown in Fig. 8(b). It can be seen that 70% of cold rolling deformations result in remarkably uniformity and significant refinement of the grain size of nt-HNASS compared with those of mt-HNASS.

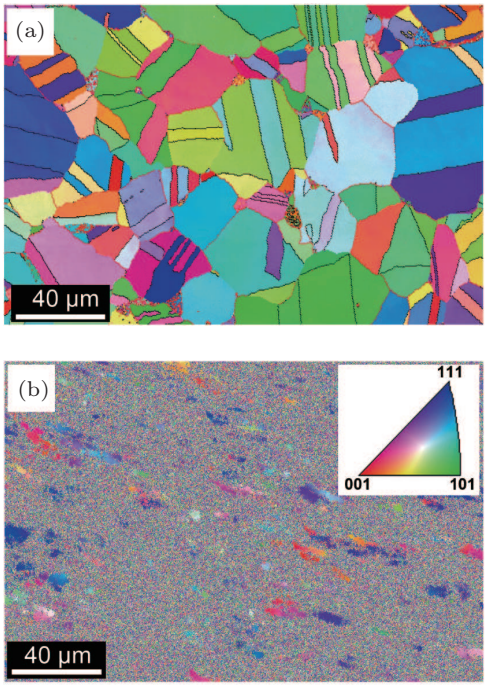


Fig. 8. (color online) IPF color maps of the mt-HNASS (a) and nt-HNASS (b) before nanoindentation tests.

The TEM observations of the microstructures of the mt-HNASS and nt-HNASS are shown in Fig. 9. The selected area electron diffraction (SAED) patterns which are plotted in an inset indicate that the HNASS is composed of twins. As shown in Fig. 9(a), the bulk twins can be seen in mt-HNASS. As shown in Fig. 9(b), a large number of nano-scale twins exist and no obvious tangles of dislocations are found in nt-HNASS. These twins are typical deformation twins formed in the cold rolling process. From statistical measurements of the twin thickness, it is found that the average twin thickness is about 14 nm for nt-HNASS. The reason for the occurrence of this high density of the nano-scale twins is that our HNASS is a sort of Cr–Mn steel that has low stacking fault energy.[21,24] These observations indicate that the cold rolling process is a new way to produce bulk nano-scale twin materials.

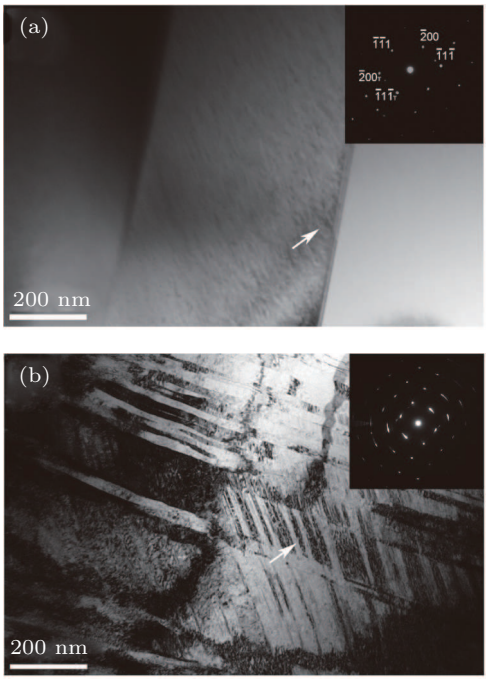


Fig. 9. TEM images of the mt-HNASS (a) and nt-HNASS (b) with the corresponding selected area diffraction patterns before nanoindentation tests.

According to the mechanistic models proposed by Asaro and Suresh,[33] the most probable sites for the dislocation nucleation are twin boundaries (TBs). It has also been demonstrated from the TEM observation that the TBs can act as dislocation sources.[34,35] Thus, dislocations can be produced from TBs in nt-HNASS in the loading regime, in a manner similar to that of the GBs in nanocrystalline fcc metals.[26] The dislocation propagation can be hindered by TBs,[36] which must be overcome by thermal activation. Furthermore, the dislocation activity will rearrange the dislocation structure at/near TBs, which also needs the assistance of atomic diffusion. So, the dislocation activity is strain rate-dependent. Considering the atomic jump or migration between dislocation core and boundaries (mainly TBs), a low strain rate can result in small dislocation accumulation and, in contrast, a high strain rate can promote large dislocation accumulation. Therefore, the accumulation of dislocations will also be dependent on $\dot{\varepsilon}_{\mathrm{L}}$, and an effective dislocation accumulation or storage can occur even at low loading strain rate in the loading regime. The higher hardness and larger m value of the nt-HNASS in Fig. 2 arises from stronger strain hardening role caused by higher storage rate of dislocations in the loading regime and the interactions between dislocations and high density of twins.

The dislocation structure is highly unstable after it has been formed in the loading regime and it can break down easily in the holding regime due to the fact that the deformation

mode changes suddenly or the continuous supporting of applied strain rate is suddenly taken away in the constant load. The stored dislocations can propagate forward and produce plastic strain (i.e., the creep strain) when they are absorbed by GBs and TBs.[37,38] This indicates that the creep process observed above is mediated mainly by the activity of dislocations. In the initial holding regime, the dislocation structures will relax rapidly and a high internal stress will thus drop off. As the holding time increases, the number of dislocations will be reduced and the stress level will drop off slowly. Therefore, the creep process mediated by the dislocation activity will slow down and a steady-state creep deformation process can occur. Thus, more significant load plateaus and higher creep rate of nt-HNASS are attributed to the rapid relaxation of the dislocation structures generated during loading regime.

Dislocations can be generated within the grains in the loading and initial holding regimes in mt-HNASS. Therefore, the effect of interaction between dislocations should be considered, which hinders the further movement of dislocations in the mt-HNASS as the holding time increases. The twins in the mt-HNASS could also affect the creep behavior, althoughn this influence may be weak due to the large thickness of twins and small number of twins. Thus, the creep deformation of mt-HNASS is mainly a result of the interaction between dislocations. Therefore, the dislocations formed in the loading and initial holding regime tangle together and the dislocation storage capacity in the larger-sized grain interior can still be effectively maintained. Under such conditions, a significant creep strain cannot be observed in mt-HNASS.

4. Conclusions

The mt-HNASS with an average twin thickness of 6.4 μm is obtained by a solution treatment at 1150 °C for 8 h, followed by water quenching. The nt-HNASS with an average twin thickness of 14 nm is prepared by cold rolling with a thickness reduction of 70%. The nanoindentation test results show that the strain rate sensitivity of the nt-HNASS is 0.0319, which is far larger than that of the mt-HNASS ($m = 0.0029$). The hardness value of the nt-HNASS are about two times as high as that of the mt-HNASS. nt-HNASS exhibits a significant load plateau and a high creep strain rate as compared with mt-HNASS. The significant creep deformation in the nt-HNASS is mainly dominated by the rapid relaxation of the dislocation structures generated during loading. The small creep deformation in the mt-HNASS is mainly due to the relatively high stability of the dislocation structures generated during loading.

Acknowledgment

The authors wish to thank Wang Huai for providing the samples of HNASS used in this study.

References

[1] Dai Q X, Yuan Z Z, Chen X and Chen K M 2009 *Mater. Sci. Eng. A* **517** 257
[2] Knutsen R D, Lang C I and Basson J A 2004 *Acta Mater.* **52** 2407
[3] Hong C M, Shi J, Sheng L Y, Cao W C, Hui W J and Dong H 2011 *Mater. Des.* **32** 3711
[4] Salahinejad E, Amini R, Marasi M and Hadianfard M J 2010 *Mater. Des.* **31** 2259
[5] Lee T H, Oh C S, Kim S J and Takaki S 2007 *Acta Mater.* **55** 3649
[6] Zhang G L, Wang J L, Liu Y F, Liu C Z and Yang S Z 2004 *Chin. Phys.* **13** 1309
[7] Zhang Y, Xie L J, Zhang J M and Xu K W 2011 *Chin. Phys. B* **20** 026102
[8] Wang H, Liu G Q and Luan J H 2012 *Acta Phys. Sin.* **61** 048102 (in Chinese)
[9] Hong C M, Shi J, Sheng L Y, Cao W Q, Hui W J and Dong H 2011 *J. Mater. Sci.* **46** 5097
[10] Fréchard S, Redjaïmia A, Lach E and Lichtenberger A 2006 *Mater. Sci. Eng. A* **415** 219
[11] Liu Y L, Jin S and Zhang Y 2012 *Chin. Phys. B* **21** 016105
[12] Simmons J W 1995 *Scripta Metallet Mater.* **32** 265
[13] Dorofeev G A, Sapegina I V, Lad'yanov V I, Pushkarev B E, Pechina E A and Prokhorov D V 2012 *The Physics of Metals and Metallography* **113** 963
[14] Yuan Z Z, Dai Q X, Cheng X N and Chen K M 2007 *Mater. Charact.* **58** 87
[15] Yuan Z Z, Dai Q X, Cheng X N, Chen K M, Pan L and Wang A D 2006 *Mater. Charact.* **56** 79
[16] Schino A D and Kenny J M 2003 *Mater. Lett.* **57** 1830
[17] Nakada N, Hirakawa N, Tsuchiyama T and Takaki S 2007 *Scr. Mater.* **57** 153
[18] Choi J Y, Ji J H, Hwang S W and Park K T 2011 *Mater. Sci. Eng. A* **528** 6012
[19] Jandová D, Řehoř J and Nový Z 2004 *J. Mater. Process. Technol.* **157–158** 523
[20] Balachandran G, Bhatia M L, Ballal N B and Rao P K 2000 *ISIJ Int.* **40** 491
[21] Saller G, Hahn K S, Scheu C and Clemens H 2006 *Mater. Sci. Eng. A* **427** 246
[22] Singh B B, Sivakumar K and Bhat T B 2009 *Int. J. Impact Eng.* **36** 611
[23] Stolyarov V V, Zhu Y T, Alexandrov I V, Lowe T C and Valiev R Z 2003 *Mater. Sci. Eng. A* **343** 43
[24] Wang S T, Yang K, Shan Y Y and Li L F 2007 *Acta Metall. Sin.* **43** 171
[25] Wang W, Yan W, Yang K, Shan Y Y and Jiang Z H 2010 *J. Mater. Eng. Perform.* **19** 1214
[26] Shen Y F, Lu L, Dao M and Suresh S 2006 *Scr. Mater.* **55** 319
[27] Dao M, Lu L, Shen Y F and Suresh S 2006 *Acta Mater.* **54** 5421
[28] Lu L, Schwaiger R, Shan Z W, Dao M, Lu K and Suresh S 2005 *Acta Mater.* **53** 2169
[29] Chen J, Shi Y N and Lu K 2005 *J. Mater. Res.* **20** 2955
[30] Lüthy H, White R A and Sherby O D 1979 *Mater. Sci. Eng.* **39** 211
[31] Coble R L 1963 *J. Appl. Phys.* **34** 1679
[32] Lucas B N and Oliver W C 1999 *Metall. Mater. Trans. A* **30** 601
[33] Asaro R J and Suresh S 2005 *Acta Mater.* **53** 3369
[34] Konopka K, Mizera J and Wyrzykowski J W 2000 *J. Mater. Process. Technol.* **99** 255
[35] Field D P, True B W, Lillo T M and Flinn J E 2004 *Mater. Sci. Eng. A* **372** 173
[36] Imran M, Hussain F, Rashid M and Ahmad S A 2012 *Chin. Phys. B* **21** 116201
[37] Mu J W, Sun S C, Jiang Z H, Lian J S and Jiang Q 2013 *Chin. Phys. B* **22** 037303
[38] Mu J W, Jiang Z H, Zheng W T, Tian H W, Lian J S and Jiang Q 2012 *J. Appl. Phys.* **111** 063506